Anomalous work function anisotropy in ternary acetylides

Joseph Z. Terdik, Károly Németh, Katherine C. Harkay, Jeffrey H. Terry, Jr., Linda Spentzouris, Daniel Velázquez, Richard Rosenberg, and George Srajer

Phys. Rev. B **86**, 035142 — Published 24 July 2012

DOI: 10.1103/PhysRevB.86.035142

Anomalous Workfunction Anisotropy in Ternary Acetylides

Joseph Z. Terdik[1], Károly Németh[1,*], Katherine C. Harkay[1], Jeffrey H. Terry, Jr.[1,2], Linda Spentzouris[1,2], Daniel Velázquez[1,2], Richard Rosenberg[1] and George Srajer[1]
[1]*Advanced Photon Source, Argonne National Laboratory, Argonne, Illinois 60439, USA and*
[2]*Illinois Institute of Technology, Chicago, IL 60616 USA*
(Dated: July 5, 2012)

Anomalous anisotropy of workfunction values in ternary alkali metal transition metal acetylides is reported. Workfunction values of some characteristic surfaces in these emerging semiconducting materials may differ by more than ≈ 2 eV as predicted by Density Functional Theory calculations. This large anisotropy is a consequence of the relative orientation of rod-like $[MC_2]_\infty$ negatively charged polymeric subunits and the surfaces, with M being a transition metal or metalloid element and C_2 refers to the acetylide ion C_2^{2-}, with the rods embedded into an alkali cation matrix. It is shown that the conversion of the seasoned Cs_2Te photo-emissive material to ternary acetylide Cs_2TeC_2 results in substantial reduction of its ≈ 3 eV workfunction down to 1.71-2.44 eV on the $Cs_2TeC_2(010)$ surface while its high quantum yield is preserved. Similar low workfunction values are predicted for other ternary acetylides as well, allowing for a broad range of applications from improved electron- and light-sources to solar cells, field emission displays, detectors and scanners.

PACS numbers:

I. INTRODUCTION

For many photo-physical applications photoemissive materials are sought after that can turn a high fraction of the incident photons into emitted electrons, i.e. materials that have a high quantum-yield. Often, the quantum-yield of these materials depends heavily on the wavelength of incident photons. For many applications, ranging from electron-guns for synchrotrons and free-electron lasers to night vision devices, high quantum-yield photoemission using visible or infrared irradiation is desirable. In electron-guns of synchrotrons and free-electron lasers, emission in the visible range is advantageous for the improved control of the shape of the emitted electron bunch that is critical for time-resolved applications. In night-vision devices a very low flux of infrared photons has to be turned into emitted electrons with a high yield in order to obtain an image as sharp as possible. Therefore there is a quest for new and improved materials with optimized quantum-yield and low-workfunction[1].

Cs_2Te has been known since the 1950-s for its high quantum-yield[2] using ultraviolet illumination with photon-energies above ≈ 3.0 eV and has been used for many decades as a primary high-yield photocathode. Besides not being photoemissive in the visible region, its other main drawback is that its surface gets oxidized in practical vacuum whereby its quantum efficiency substantially reduces[3]. Despite this disadvantage, Cs_2Te still has 20-30 times longer operational lifetime than competing multi-alkali antimonide photocathodes, such as K_2CsSb and $(Cs)Na_3KSb$, especially when operated in radio-frequency accelerating cavities[3].

In the process of attempting to design modifications of Cs_2Te with lowered workfunction and preserved high quantum-yield we have considered the effects of small gas molecules on Cs_2Te surfaces. Such effects have been studied by di Bona *et al.*[3], using small gas molecules occurring in vacuum, such as O_2, N_2, CO_2, CO and CH_4. It occurred to us that the effect of another small gas molecule, acetylene (C_2H_2) has not been considered yet, despite the potentially interesting reactions between C_2H_2 and Cs_2Te. C_2H_2 is widely used for welding (not in accelerators though) and it might occur in accelerator-vacuums as well, in trace amounts. It is an acidic compound and prefers to decompose to acetylide anion C_2^{2-} and to $2H^+$ in the presence of a base. Based on the acidic character of C_2H_2, one might investigate the working hypothesis that the reaction of

$$Cs_2Te(cr) + C_2H_2(g) \rightarrow Cs_2TeC_2(cr) + H_2(g) \qquad (1)$$

would produce a ternary acetylide Cs_2TeC_2 whereby the oxidation number of Te would change from -2 to 0 and that of H from +1 to 0, with (cr) denoting crystal and (g)

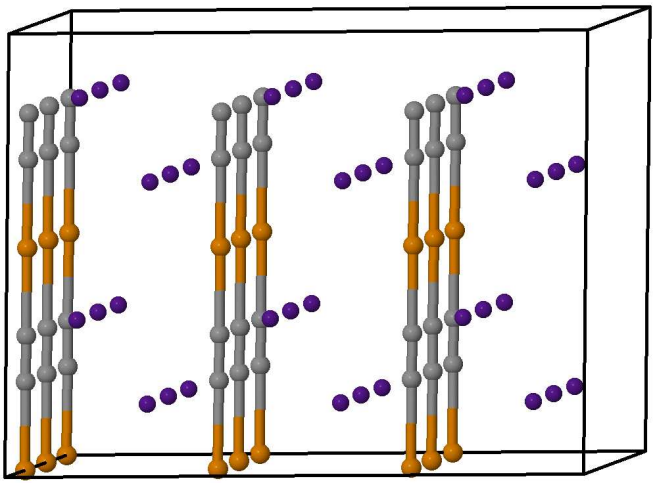

FIG. 1: A side-view of the 3x3x2 supercell of the hexagonal unit cell of Cs_2TeC_2. Bronze spheres denote Te, grey ones C, dark-purple ones Cs. Notice the $[TeC_2]_\infty$ rods.

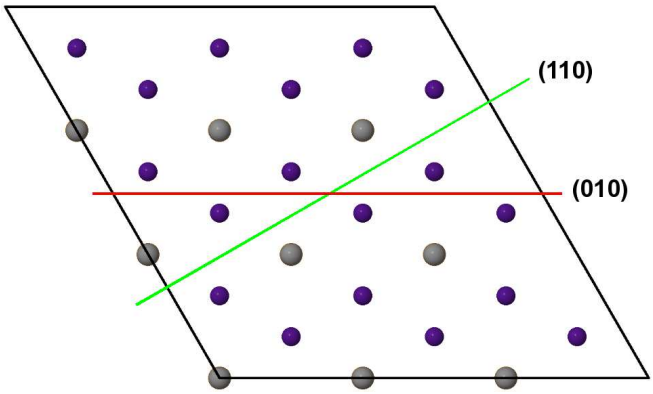

FIG. 2: A top-down view of a 3x3x2 supercell of the hexagonal unit cell of Cs_2TeC_2. Color codes are identical with those in Fig. 1. The $[TeC_2]_\infty$ rod-like substructures are running perpendicularly to the plane viewed. The red line indicates the energetically preferred cleavage-plane for the (010) surface running between two layers of Cs atoms, parallel with the rods, while the green line refers to the preferred cleavage-plane for the (110) surface that involves $[TeC_2]_\infty$ rods directly exposed on the surface. Note that the (010) and (100) planes are identical.

gas phase. Interestingly, the class of ternary (i.e. three-component) acetylides indeed exists, involving already synthesized members with the general formula of A_2MC_2 with A∈[Na,K,Rb,Cs] and M∈[Pd,Pt], and the oxidation number of the metal M in them is zero[4,5]. All existing compounds of the A_2MC_2 formula have a hexagonal unit cell with rod-like $[MC_2]_\infty$ substructures running parallel with the main crystallographic axis, and very similar distribution of alkali atoms around the $[MC_2]_\infty$ rods, just as indicated in Figs. 1 and 2. All known A_2MC_2 materials are colored semiconductors with 2.1-2.8 eV direct band-gaps[5]. The other class of ternary acetylides with synthesized members contains only a single alkali atom and has the formula of AMC_2[6] with the $[MC_2]_\infty$ rods adopting 3 different kinds of rod-packings[7].

II. METHODOLOGY

Adopting the structure of the unit cell of Na_2PdC_2 and substituting Na with Cs and Pd with Te we have carried out a full crystal structure (lattice parameters and atomic fractional coordinates) optimization using Density Functional Theory (DFT), without any symmetry and point group constraints on the translational unit cell. We have used the PWSCF-code[8], plane-wave representation of wave-functions with 80 Rydbergs wavefunction-cutoff, the PBE exchange-correlation functional[9] in conjunction with norm-conserving pseudopotentials for Cs, Na and Te and ultrasoft ones for the other elements as available in the PWSCF distribution. The k-space grids were at least 6×6×6 large for optimizations, the residual forces on fractional coordinates were less than 4×10^{-4} Ry/au, residual pressure on the unit cell less than 1 kbar. For validation of the DFT-based methodology, we have calculated known structural parameters and workfunctions of compounds with similar composition, achieving good agreement between computed and experimental values as indicated in Tables I, II and III. Note that in some cases, like Na_2PdC_2 and Cs_2PdC_2 the difference between calculated and experimental a and b lattice parameters (rod distances) was about 3-3.5%, significantly larger than that for the c lattice parameter (<1%), which we have accepted on the basis that the inter-rod interactions are more difficult to accurately predict, similarly to general intermolecular interactions. The workfunction calculations were based on slabs of at least 30 Å width separated by vacuum layers up to 120 Å following the methodology of Ref. 10. For additional validation of the use of the PBE functional here, we have compared the direct bandgaps of Na_2PdC_2 and Cs_2PdC_2 to experimental data. Experimental direct bandgaps of Na_2PdC_2, K_2PdC_2 and Rb_2PdC_2 are at 2.09, 2.55 and 2.77 eV, that of Cs_2PdC_2 is estimated to be slightly greater than that of Rb_2PdC_2[5]. Our PBE calculations predict the lowest energy direct transitions between 1.2-1.8 eV for Na_2PdC_2 (near the H point) and 1.7-2.6 eV for Cs_2PdC_2 (near the H and K points), as shown in Fig. 3. The overall characteristics of these bands is similar to those calculated previously for ternary acetylides, e.g. in Refs. 5, 7 and 12. Band gaps of bulk Cs_2Te, Cs_2TeC_2 and Na_2TeC_2 have been predicted to be between 1.8-2.0 eV, using the PBE functional (Fig. 4).

We have also calculated the optical absorption spectra of some ternary acetylides and Cs_2Te (Figs. 5 and 6) in the Random Phase Approximation (RPA) using the YAMBO-code[11]. All optical absorption calculations have been performed with a resolution of $\Delta k < 0.1$ Å^{-1}, and a Gaussian broadening of 0.03 Ry. Note that for maximum absorption the polarization of the light was parallel with rods in the ternary acetylides and parallel with the crystallographic c-axis in Cs_2Te (see Fig. 7). Due to the lack of norm-conserving pseudopotential for Pd, optical absorption spectra of Na_2PdC_2 and Cs_2PdC_2 could not be calculated. In order to associate these gaps with transition probabilities, a crude approximation of these spectra using only planewaves with G=0 wave-vectors was attempted. It indicates absorption maxima at 1.8 and 2.6 eV for Na_2PdC_2 and Cs_2PdC_2, respectively (Fig. 5). Unexpectedly, PBE0[13] calculations at the same geometries result in about 1.0 eV larger gaps than the experimental ones.

III. RESULTS AND DISCUSSION

The optimization reveals that Cs_2TeC_2 has a very similar structure to other compounds of the A_2MC_2 class. Our DFT calculations predict that the electronic energy change in Eq. 1 is $\Delta E = +1.1$ eV per Cs_2TeC_2 unit,

TABLE I: Validation of the a, b and c lattice parameters on several test systems using the PBE density functional, as described in the discussion. Orthorhombic and hexagonal Cs_2C_2 are denoted as o-Cs_2C_2 and h-Cs_2C_2, respectively, with structural parameters not very accurately determined due to the coexistence of the two phases at any temperature.

Compound, space-group & reference	Lattice Parameters (Å) EXPT a	EXPT b	EXPT c	DFT a	DFT b	DFT c
Cs ($Im\overline{3}m$)[14]	6.067	6.067	6.067	6.067	6.067	6.067
Te ($P3_121$)[15]	4.526	4.526	5.920	4.458	4.458	5.925
Cs_2Te (Pnma)[16]	9.512	5.838	11.748	9.558	5.832	11.750
C ($Fd\overline{3}m$)[17]	3.567	3.567	3.567	3.573	3.573	3.573
Na_2C_2 ($I4_1/acd$)[18]	6.778	6.778	12.740	6.941	6.941	13.027
o-Cs_2C_2 (Pnma)[19]	9.545	5.001	10.374	9.826	5.061	10.491
h-Cs_2C_2 ($P\overline{6}2m$)[19]	8.637	8.637	5.574	8.728	8.728	6.048
$CsAgC_2$($P4_2mmc$)[6]	5.247	5.247	8.528	5.317	5.317	9.036
Na_2PdC_2 ($P\overline{3}m1$)[5]	4.464	4.464	5.266	4.632	4.632	5.284
Cs_2PdC_2 ($P\overline{3}m1$)[4]	5.624	5.624	5.298	5.804	5.804	5.265
Na_2TeC_2 ($P\overline{3}m1$)	-	-	-	4.767	4.767	6.102
Cs_2TeC_2 ($P\overline{3}m1$)	-	-	-	5.820	5.820	6.152

TABLE II: Validation of C-C and M-C distances (M is transition-metal or metalloid element).

Compound, Space-group & ref.	d(C-C) (Å) EXPT	d(C-C) (Å) DFT	d(M-C) (Å) EXPT	d(M-C) (Å) DFT
C ($Fd\overline{3}m$)[17]	1.544	1.547	-	-
C_2H_2 (gas)[20]	1.203	1.203	-	-
Na_2C_2 (I41/acd)[18]	1.204	1.261	-	-
o-Cs_2C_2 (Pnma)[19]	1.385	1.269	-	-
h-Cs_2C_2 ($P\overline{6}2m$)[19]	0.934	1.267	-	-
$CsAgC_2$ ($P4_2mmc$)[6]	1.216	1.249	2.016	2.034
Na_2PdC_2 ($P\overline{3}m1$)[5]	1.262	1.271	2.019	2.006
Cs_2PdC_2 ($P\overline{3}m1$)[4]	1.260	1.280	2.019	1.993
Na_2TeC_2 ($P\overline{3}m1$)	-	1.259	-	2.422
Cs_2TeC_2 ($P\overline{3}m1$)	-	1.257	-	2.452

TABLE III: Experimental and calculated (DFT) properties of photoemissive surfaces of validation materials: workfunctions (Φ), bandgaps at the Γ-point $E_g(\Gamma)$ and surface energies (σ).

Compound surface	Φ (eV) EXPT	Φ (eV) DFT	$E_g(\Gamma)(eV)$ DFT	σ (eV/Å^2) DFT
Cs(100)	2.14[21]	2.00	0.29	0.005
Te(001)	4.95[21]	5.02	0.54	0.036
Cs_2Te(001)	2.90-3.0[22]	3.08	0.77	0.015
Cs_2Te(010)	2.90-3.0[22]	2.90	1.04	0.014
(Cs)Na_3KSb	1.55[23]	-	-	-
K_2CsSb	1.9-2.1[24,25]	-	-	-

TABLE IV: Calculated (DFT) properties of photoemissive surfaces of acetylide compounds: workfunctions (Φ), bandgaps at the Γ-point $E_g(\Gamma)$ and surface energies (σ). Relaxed slabs refer to the relaxation of unrelaxed ones with the central 2 layers fixed. For h-Cs_2C_2(001) and Na_2TeC_2(010), $E_g(\Gamma) \approx 0.05$ eV has been found for a single band above E_F as well.

Compound and surface	unrelaxed Φ (eV)	unrelaxed $E_g(\Gamma)$ (eV)	unrelaxed σ (eV/Å^2)	relaxed Φ (eV)	relaxed $E_g(\Gamma)$ (eV)	relaxed σ (eV/Å^2)
o-Cs_2C_2(010)	2.80	1.25	0.023	-	-	-
h-Cs_2C_2(001)	2.56	1.14	0.027	-	-	-
Na_2PdC_2(001)	3.58	1.13	0.067	-	-	-
Na_2PdC_2(110)	3.73	1.65	0.029	4.17	2.34	0.024
Na_2PdC_2(010)	2.65	1.91	0.019	2.68	2.45	0.017
Cs_2PdC_2(001)	2.90	1.43	0.046	-	-	-
Cs_2PdC_2(110)	2.73	0.88	0.026	2.73	1.16	0.022
Cs_2PdC_2(010)	1.33	0.78	0.015	2.03	1.74	0.013
Na_2TeC_2(001)	3.40	1.03	0.029	-	-	-
Na_2TeC_2(110)	3.80	0.91	0.025	4.67	2.04	0.009
Na_2TeC_2(010)	2.75	1.43	0.015	2.68	1.34	0.015
Cs_2TeC_2(001)	3.71	1.86	0.022	-	-	-
Cs_2TeC_2(110)	2.77	0.77	0.020	2.98	1.38	0.019
Cs_2TeC_2(010)	1.71	1.00	0.013	2.44	1.63	0.009

while that in the alternative reaction of

$$Cs_2C_2(cr) + Te(cr) \rightarrow Cs_2TeC_2(cr) \qquad (2)$$

is ΔE = -0.95 eV, indicating the stability of the Cs_2TeC_2 crystal and an alternative synthesis route. In fact the synthesis in Eq. 2 is analogous to that of already existing A_2MC_2 compounds[5]. The predicted stability of a ternary acetylide with metalloid element (Te) instead of a transition metal for M in the A_2MC_2 formula is indicative of potential extension of this class of materials with metalloids, while preserving the peculiar rod-like $[MC_2]_\infty$ substructures. Our analysis at this point cannot exclude the existence of other structures for Cs_2TeC_2. We have attempted to start the optimization of a 5 atomic unit cell of Cs_2TeC_2 from several randomly chosen initial lattice parameters and atomic positions. In all cases the formation of $[TeC_2]_\infty$ rods was evident after a few hundred steps. Here we have relied on the fact that A_2MC_2 compounds have been found only with hexagonal rod packing so far. Also, the structure of h-Cs_2C_2 already contains the hexagonal rod-packing of the C_2 units leaving place for intercalatable atoms, such as Te, or transition metals, between neighboring C_2-s along a rod.

One should also note that the linear chains of carbon atoms, $[C_2]_\infty$ with alternating C-C and C≡C bonds (polycarbyne) or with uniform C=C bonds (cumulenes, polyallenes), have long been a subject of theoretical and materials science interest[26,27]. However, unlike their hydrogenated analogue, $[C_2H_2]_\infty$ polyacetylene, containing alternating C-C and C=C bonds, famous for high electrical conductivity on the order of that of silver when doped[28,29], $[C_2]_\infty$ could not have been synthesized un-

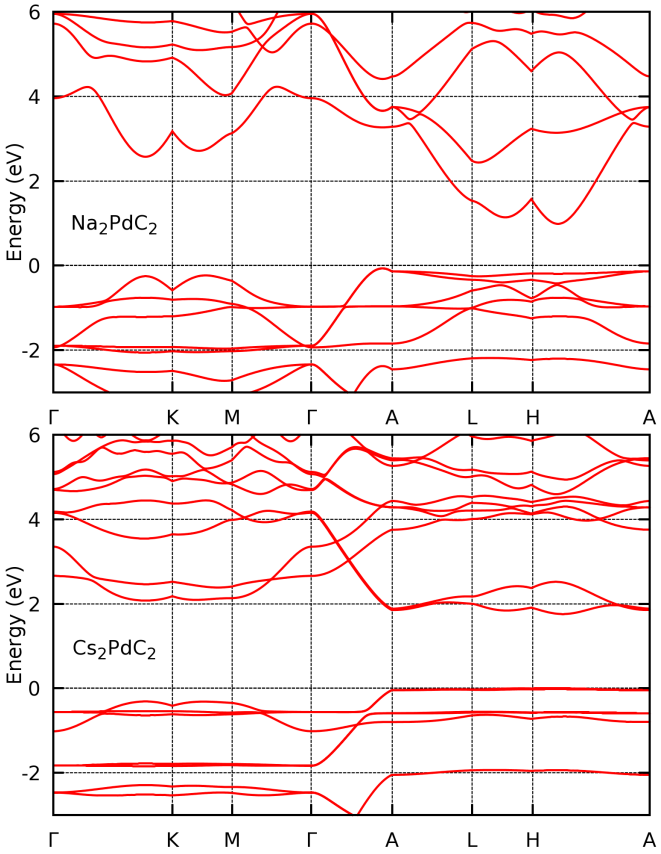

FIG. 3: Bandstructures of Na_2PdC_2 and Cs_2PdC_2 using the PBE[9] exchange-correlation functional. The k-space was 14×14×14 large. The Fermi energy is at 0 eV. Flat bands are characteristic for ternary acetylides.

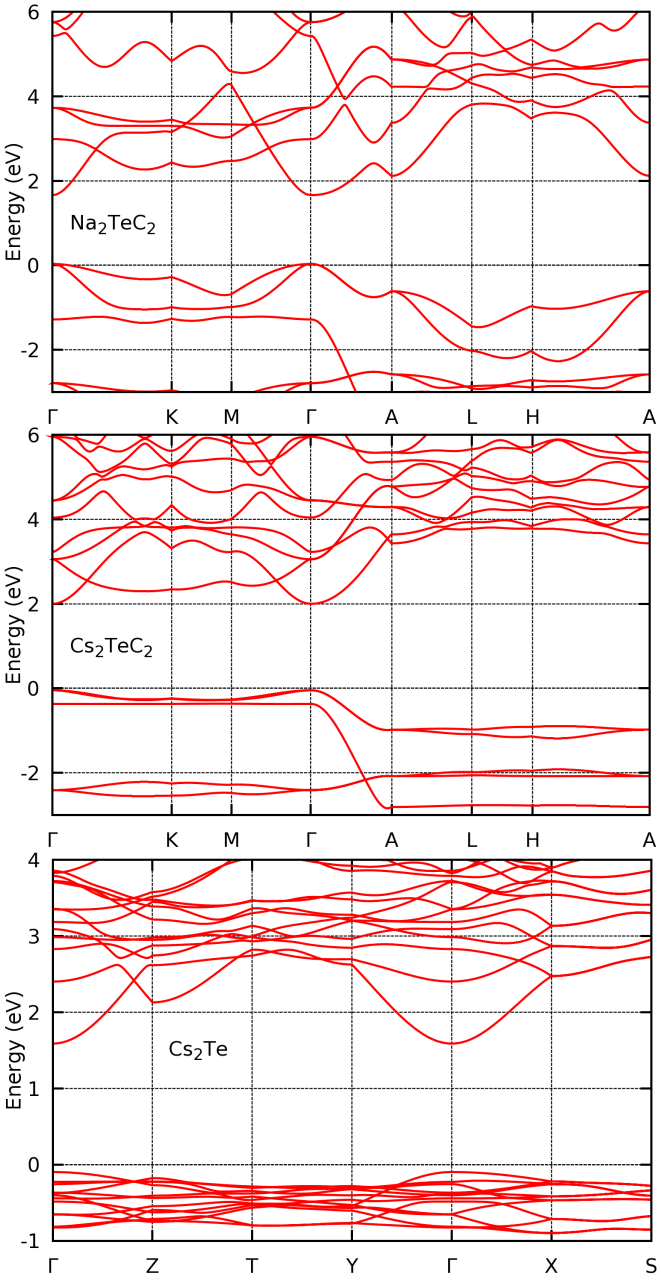

FIG. 4: Bandstructures of Na_2TeC_2, Cs_2TeC_2 and Cs_2Te, using the PBE[9] exchange-correlation functional. The k-space was 14×14×14 large. The Fermi energy is at 0 eV.

til a decade ago, proving the existence of $[C_2]_n$ with n∈≈[200,300][30]. Interestingly, the efficient synthesis of $[C_2]_n$ involves copper-acetylides[30]. Furthermore, copper-acetylides can also be used as the starting material for their synthesis[31], pointing to the intimate relationship of the rod-like $[MC_2]_\infty$ substructures in ternary-acetylides A_2MC_2 and AMC_2 to linear carbon chains. Copper-acetylide molecules are also studied for their self assembly into extremely thin nanowires[32]. It is also important to note that while transition-metal acetylides are known explosives, their alkalinated versions AMC_2 and A_2MC_2 are not explosive at all and can survive heating up to ≈ 500-600 °C and grinding[5,33].

As it is indicated in Table IV, the workfunctions of different surfaces of Cs_2TeC_2 have largely different values. Concerning the three most important surfaces (Fig. 2), there is a ≈ 1 eV decrease as one goes from (001) through (110) to (010) in each step, with workfunctions of 3.71, 2.77 and 1.71 eV, and surface energies of 0.022, 0.020 and 0.013 eV/Å^2, respectively, for the unrelaxed surfaces. Relaxed surfaces have somewhat greater workfunction values, but still allowing for emission in the visible spectrum. Relaxation of the surface layers greatly influences the unoccupied bands, while the occupied ones change significantly less, as indicated in Fig. 8. Also note that the total energy differences between relaxed and unrelaxed surfaces are small, for example they are only 0.3 eV for a whole Cs_2TeC_2(010) slab, i.e. about 0.01 eV/atom in the top surface layers which allows for thermal population of a great variety of surface structures at room temperature. In Cs_2TeC_2(010) and Na_2TeC_2(010) surface relaxations may break the $[TeC_2]_\infty$ rods, while the rods stay intact in Pd (or other transition metal) based ternary acetylides. In Cs_2PdC_2(010) and Na_2PdC_2(010) the rods provide quasi rails along which Cs-s and Na-s

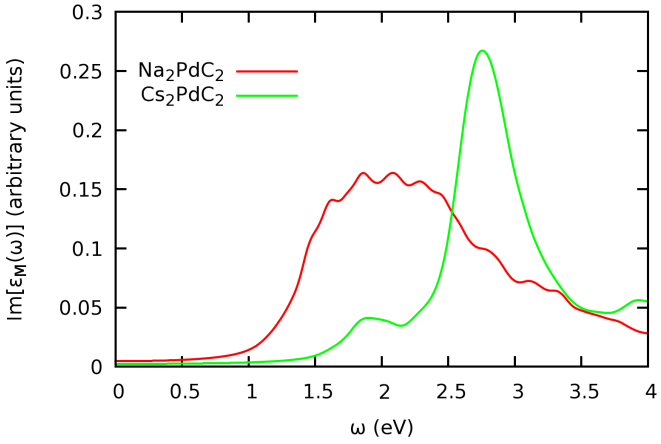

FIG. 5: Optical absorption spectra of bulk Na_2PdC_2 and Cs_2PdC_2 from the imaginary part of the macroscopic dielectric function $\varepsilon_M(\omega)$. Only the G=0 planewaves were used to calculate intensities in the RPA approximation. The polarization vector of the light is along the main crystallographic axis (along the $[PdC_2]_\infty$ chains).

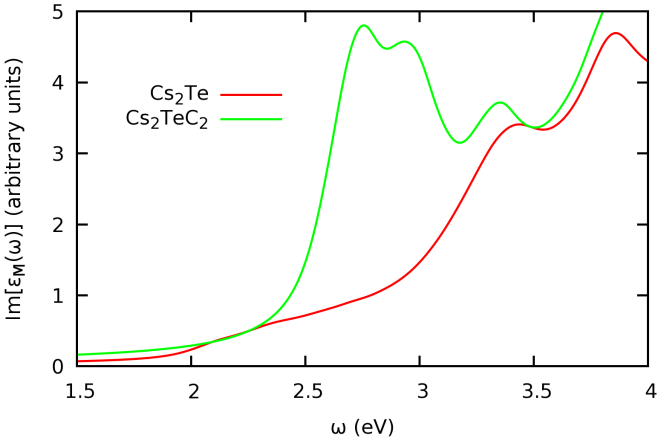

FIG. 6: Optical absorption spectra of bulk Cs_2Te and Cs_2TeC_2 from the imaginary part of the macroscopic dielectric function $\varepsilon_M(\omega)$. The 4000 lowest energy planewaves were used to calculate intensities in the RPA approximation. The polarization vector of the light is along the main crystallographic axis (along the $[TeC_2]_\infty$ chains and the c-axis of Cs_2Te).

can easily move due to thermal motion. This is also in accordance with the anomalous broadening of peaks in the x-ray powder spectra of ternary acetylides[7]. Such an anomalous anisotropy of workfunction values is highly unusual and represents a broad range of workfunction choice within a single material, allowing for emission in ultraviolet, visible and near infrared radiation. The lowest surface cleavage energy Cs_2TeC_2 surface, (010), has a similar surface energy as those of Cs_2Te surfaces; it is, however, associated with a much lower (by $\approx$ 1.3 eV) workfunction. The highly anisotropic properties of Cs_2TeC_2 are due to the relative orientation of the rod-like $[TeC_2]_\infty$ substructures and the surfaces. Surface energies reveal that cutting the rods by cleaving the M-C bonds ((001) surface) is energetically disadvantageous, and it is also disadvantageous to allow for rods to be directly exposed on the surface ((110) surface), while cleavage between Cs atoms with rods embedded under the surface is the most energetically favorable construct ((010) surface). While numerous variants of surface coverages may exist at different temperatures that expose or cover rods by Cs on the surface, here we do not go beyond a single surface unit to study the energetics of surfaces. The sticking of Cs to these surfaces may be a similarly important issue here as in the case of cesiated III/V semiconductor surfaces (e.g. GaAs)[34]. As the rods are twice negatively charged per MC_2 unit, we expect that the sticking of Cs cations would be relatively strong.

High anisotropy can be observed in Na_2PdC_2, Na_2TeC_2 and Cs_2PdC_2 as well, with somewhat smaller, 1.1-1.6 eV difference between the extremal surfaces. The type of the alkali atom very sensitively influences the workfunctions: substituting Na with Cs results in more than 1 eV reduction of the workfunction on the (110) and (010) surfaces independently from the type of the $[MC_2]_\infty$ chain, even though the M-C bonding in these chains is very different. One has to note that the Pd-C distance is significantly shorter than the Te-C in these compounds, 2.01 Å vs. 2.45 Å, respectively, while Te and Pd have very similar covalent radii of $\approx$ 1.4 Å[35]. The (001) surface energies also indicate a much stronger Pd-C bond than Te-C one. While there is a σ-bond in both Pd-C and Te-C links between the $2sp^1$ hybrid orbital of the C atom and the $5sp^1$ hybrids of Pd and Te (all oriented along the M-C-C line) the Pd-C link is further strengthened by strong back-donation of Pd 4d shell electrons to the antibonding π-orbitals of the C_2^{2-} ions, also associated with lengthening of the C-C bond[5]. Also note that Cs_2Te (and also Cs_2TeC_2) has the advantage over the formerly mentioned multi-alkali-antimonides that Cs is better bound in them allowing for longer operational lifetime[1]. Another interesting comparison can be made to amorphous cesiated carbon films obtained from the co-deposition of high-energy negatively charged carbon ions and Cs on silicon substrates, as the low, $\approx$ 1.1 eV workfunction in them might be associated with increased acetylide ion concentration. However, there is no available data of how well Cs is bound in these systems[36].

In order to estimate the quantum-yield of Cs_2TeC_2 relative to Cs_2Te, we have calculated their optical absorption spectra (Fig. 6) using the lowest energy 4000 planewaves at which the spectrum becomes saturated against further increase of the number of planewaves. The spectra indicate that acetylation of Cs_2Te shifts its first absorption peak in the visible region to 2.7 eV, while preserving the same absorption intensity. This comparison suggests that Cs_2TeC_2 may have similarly high quantum efficiency as that of Cs_2Te, however, even for visible and potentially also for near infrared photons. The

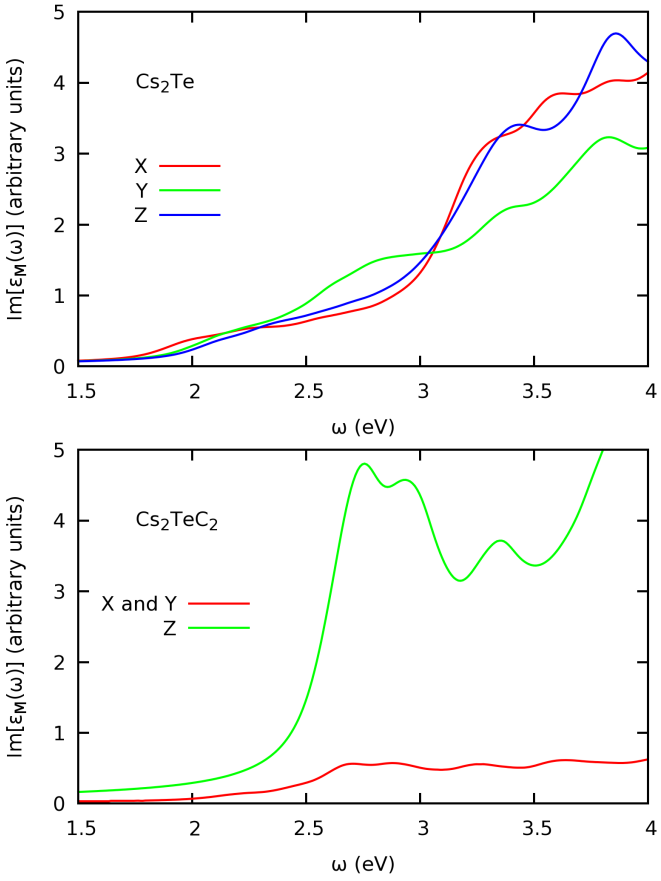

FIG. 7: Dependence of the optical absorption spectra of bulk Cs_2Te and Cs_2TeC_2 on the polarization of the incident light. The z-direction is along the main crystallographic axis (c-axis), which is parallel with the $[TeC_2]_\infty$ chains in Cs_2TeC_2. While absorption in Cs_2TeC_2 is highly anisotropic, with ≈ 9 times higher values for the z-direction than for the x and y ones, there is no significant anisotropy of absorption in Cs_2Te. Similar anisotropy can be seen in Na_2TeC_2 as well, and likely in all ternary acetylides, due to the electric dipoles along the $[MC_2]_\infty$ chains.

bandgaps at the Γ point of Cs_2TeC_2 surfaces (see Table IV) also support that photon-energies near the workfunction are sufficient to induce emission in this material. An interesting characteristics of ternary acetylides is the extensive presence of flat bands (see Figs. 3 and 4). While there are some flat band parts in Cs_2Te as well, such a feauture is much more characteristic for ternary acetylides. Flat bands greatly increase the density of states for some spectral regions thus they contribute to increased absorption of light. Interestingly, not only the workfunctions of these materials show high anisotropy, but also their optical absorption (see Fig. 7). The optical absorption is almost a magnitude greater when the light's polarization vector is parallel with the $[MC_2]_\infty$ rods. This property can allow for example for the generation of pulsed electron beams when these surfaces are illuminated by circularly polarized light. Several other optical applications can be envisioned based on the anisotropy of optical absorption in ternary acetylides, such as polar-filters and optical switching elements.

It is also important to call attention to the rest of the ternary acetylides as valuable photoemissive materials. For example the already synthesized $Cs_2PdC_2(010)$[4] material is predicted here to have a very low 1.33-2.03 eV workfunction even smaller than that of $Cs_2TeC_2(010)$ and a similar density of states.

While it may be difficult to lower the workfunction into the infrared spectral domain (below 1.5 eV), multiphoton absorption of infrared light may still provide a way to photo-emission in this domain as well. Strong multiphoton absorption of organic and inorganic compounds with acetylide units is well known[37], for example in platinum acetylides[38], the analogy suggests that multiphoton absorption may be strong in ternary acetylides as well. Multiphoton absorption happens via simultaneous absorption of multiple photons without the need of real intermediate states as opposed to cascaded multiple step one-photon absorptions[37]. These latter ones are also possible in ternary acetylides as there are surface states 1-1.5 eV above the Fermi level as indicated in Fig. 8.

Emission from $A_2MC_2(001)$ surfaces (rods perpendicular to surface) may especially be suitable for generating low transverse emittance electron beams[39] as excited electrons are expected to be guided along the $[MC_2]_\infty$ rods while traveling from inside the bulk of the cathode towards the surface whereby not being scattered side-wise, analogously to needle-array cathodes of field emission[40].

IV. CONCLUSIONS

In the present work we have demonstrated unique photoemissive properties of ternary acetylides, such as low workfunctions, high workfunction and optical absorption anisotropy and high quantum yield. We have also demonstrated how the acetylation of the seasoned Cs_2Te photocathode material leads to significantly lowered workfunction while preserving its high quantum yield.

V. ACKNOWLEDGEMENTS

The authors gratefully acknowledge A. Zholents and K. Attenkofer (APS/Argonne) for helpful discussions and thank NERSC (U.S. DOE DE-AC02-05CH11231) for the use of computational resources. J. Z. Terdik thanks A. Zholents for support. This research was supported by the U.S. DOE Office of Science, under contract No. DE-AC02-06CH11357, and also by the National Science Foundation (No. PHY-0969989).

∗ Nemeth@ANL.Gov

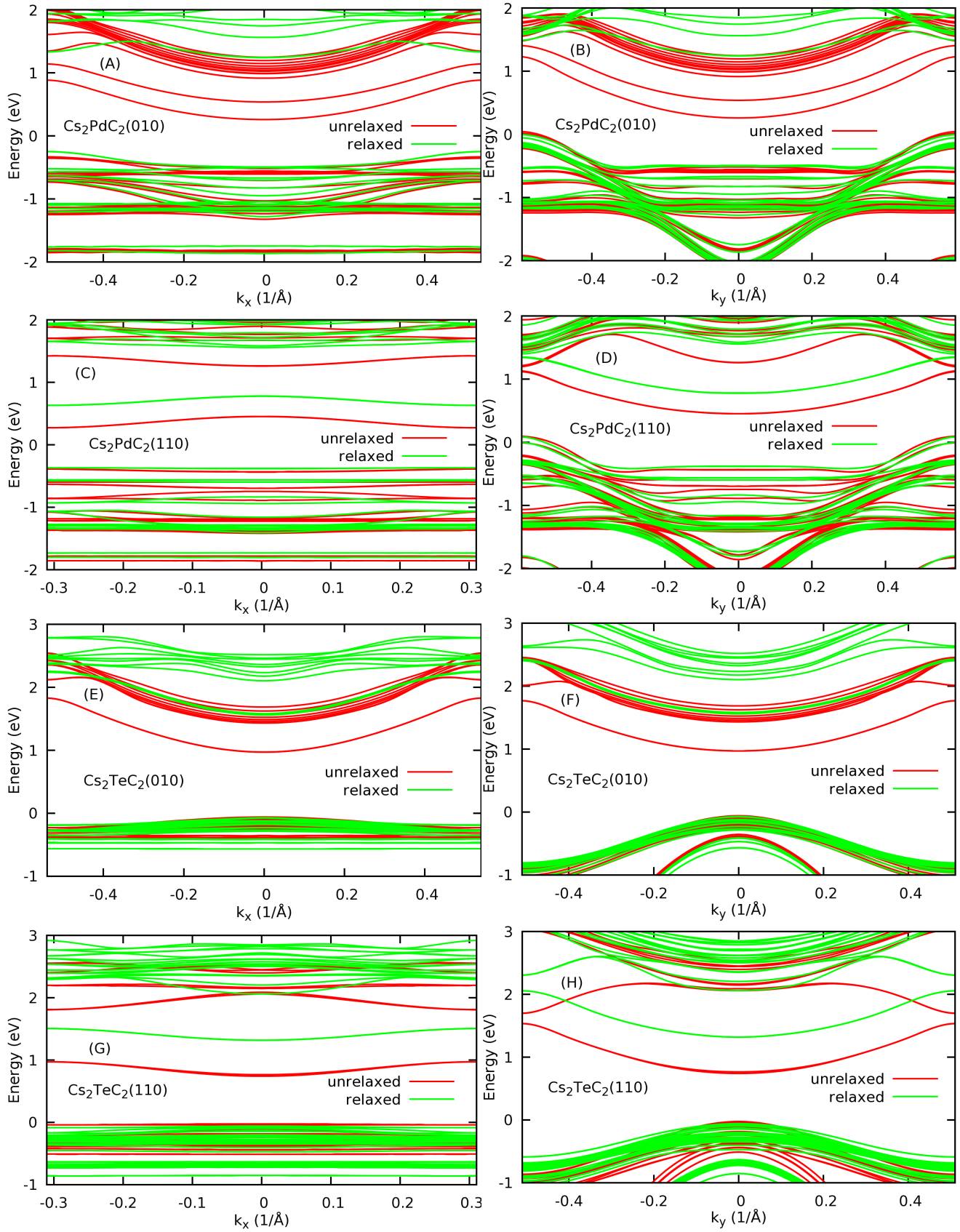

FIG. 8: Electronic bands of the slabs of the (010) and (110) surfaces of Cs_2PdC_2 and Cs_2TeC_2 along the two orthogonal reciprocal surface lattice vectors k_x (panels A, C, E and G) and k_y (panels B, D, F and H). The $[MC_2]_\infty$ rods are parallel with the y direction for all (010) and (110) surface slabs. Bands at both relaxed (green) and unrelaxed (red) slabs are shown. The Fermi energy is at 0.

[1] D. H. Dowell *et.al*, Nuclear Instruments and Methods in Physics Research A **622**, 685 (2010).
[2] E. Taft and L. Apker, J. Opt. Soc. Am. **43**, 81 (1953).
[3] A. di Bona *et.al*, J. Appl. Phys. **80**, 3024 (1996).
[4] U. Ruschewitz, Z. Anorg. Allg. Chem. **627**, 1231 (2001).
[5] H. Billetter *et.al*, Z. Anorg. Allg. Chem. **636**, 1834 (2010).
[6] W. Kockelmann and U. Ruschewitz, Angew. Chem. Int. ed. **38**, 3495 (1999).
[7] U. Ruschewitz , Z. Anorg. Allg. Chem. **632**, 705 (2006).
[8] P. Gianozzi *et.al*, J. Phys.: Condens. Matter **21**, 395502 (2009), http://www.quantum-espresso.org.
[9] J. P. Perdew *et.al*, Phys. Rev. Lett. **77**, 3865 (1996).
[10] C. J. Fall *et.al*, J. Phys.: Cond. Mat. **11**, 2689 (1999).
[11] A. Marini *et.al*, Comp. Phys. Comm. **180**, 1392 (2009), http://www.yambo-code.org.
[12] S. Hemmersbach *et.al*, Chem. Eur. J. **7**, 1952 (2001).
[13] C. Adamo *et.al*, J. Chem. Phys. **110**, 6158 (1999).
[14] C. S. Barrett, Acta Cryst. **9**, 671 (1956).
[15] N. Bouad *et.al*, J. Solid State Chem. **173**, 189 (2003).
[16] I. Schewe-Miller *et.al*, Golden Book of Phase Transitions 5, Wroclaw **1**, 123 (2002).
[17] M. E. Straumanis *et.al*, J. Am. Chem. Soc. **73**, 5643 (1951).
[18] S. Hemmersbach *et.al*, Z. Anorg. Allg. Chem. **625**, 1440 (1999).
[19] U. Ruschewitz *et.al*, Z. Anorg. Allg. Chem. **627**, 513 (2001).
[20] John Overend , Trans. Faraday Soc. **56**, 310 (1960).
[21] H. B. Michaelson, J. Appl. Phys. **48**, 4729 (1977).
[22] S. Lederer *et.al*, in *Proc. FEL 2007* (2007), p. 457.
[23] A. Sommer, *Photoemissive Materials* (John Wiley & Sons, New York, 1968).
[24] I. Bazarov *et.al*, Appl. Phys. Lett. **98**, 224101 (2011).
[25] T. Vecchione *et.al*, Appl. Phys. Lett. **99**, 034103 (2011).
[26] S. Roth and D. Carroll, *One Dimensional Metals: conjugated polymers, organic crystals, carbon nanotubes* (Wiley-VCH, Weinheim, 2004).
[27] F. Diederich, in *Modern Acetylene Chemistry*, edited by P. J. Stang and F. Diederich (VCH, Weinheim, 1995).
[28] C. K. Chiang *et.al*, J. Am. Chem. Soc. **100**, 1013 (1978).
[29] Nobel Prize in Chemistry, 2000, to A. J. Heeger, A. G. MacDiarmid and H. Shirakawa.
[30] F. Cataldo, Polymer International **44**, 191 (1997).
[31] F. Cataldo, Polymer International **48**, 15 (1999).
[32] K. Judai *et.al*, Adv. Mater. **18**, 2842 (2006).
[33] R. Buschbeck *et.al*, Coordination Chemistry Reviews **255**, 241 (2011).
[34] M. Besançon *et.al*, Surface Science **236**, 23 (1990).
[35] C. Beatriz *et.al*, Dalton Trans. **21**, 2832 (2008).
[36] Y. W. Ko and S. I. Kim, J. Appl. Phys. **82**, 2631 (1997).
[37] Guang S. He *et.al*, Chem. Rev. **108**, 1245 (2008).
[38] K. Sonogashira *et.al*, J. Organomet. Chem. **145**, 101 (1978).
[39] K. Németh *et.al*, Phys. Rev. Lett. **104**, 046801 (2010).
[40] R. Ganter *et.al*, Phys. Rev. Lett. **100**, 064801 (2008).